Petäjäjärvi et al. EURASIP Journal on Wireless Communications and Networking (2016) 2016:179
DOI 10.1186/s13638-016-0674-5

EURASIP Journal on Wireless Communications and Networking

RESEARCH Open Access

On the human body communications: wake-up receiver design and channel characterization

Juha Petäjäjärvi*, Konstantin Mikhaylov, Risto Vuohtoniemi, Heikki Karvonen and Jari Iinatti

Abstract

By modulating the electric field induced to a human body, it is possible to transfer data wirelessly using the body as a transmission medium. This method is referred to as human body communication (HBC), which has multiple advantages in comparison with the traditional radio frequency (RF) communication. First, it alleviates the traffic load from the radio channels, which are becoming more and more congested, as the number of connected wireless devices increases rapidly. Second, HBC can potentially provide higher security than traditional RF communication since the electric field stays in the vicinity of a human body, which makes eavesdropping more challenging. Third, the attenuation in the HBC frequency band is lower than in bands used by the other radio technologies for wireless body area networks. To improve energy efficiency in HBC, one approach is to utilize a wake-up receiver (WUR). The WUR is continuously listening for a pre-defined wake-up signal, which activates the other electric circuitry (e.g., sensing, processing, and communication). The use of WURs can significantly reduce the energy consumption and increase the lifetime of the sensing applications. In this work, we propose a superregenerative WUR solution which employs self-quenching and loose synchronization method and operating at sufficiently low (1.25 kbps) data rate in order to obtain high sensitivity while keeping the energy consumption low. This enables to achieve sensitivity of −97 dBm for 10^{-3} bit error rate while consuming only 40 μW. The details of the design and the performance evaluation results of the proposed solution are in the paper. Also, the paper reports the results of the practical measurements characterizing the impact of the electrode location on the path loss in an HBC channel. The presented results show that the proposed system can potentially enable communication between two any points on the body with low transmit power.

Keywords: HBC, IoT, Low power, Pulse width modulation, Selectivity, Sensitivity, Wake-up signal, WBAN

1 Introduction

Wireless body area networks (WBAN) have been under an active research for more than a decade now and are about to evolve from a concept to real applications and products. To enable this, during the recent years significant research efforts have been put in solving one of the major challenges of these systems, namely the way to provide high energy efficiency. Although there are multiple aspects affecting energy consumption of WBANs (including, e.g., the hardware design of sensors, actuators, and processing units, as well as the algorithms and data processing techniques), undoubtedly the communication is one of the major contributors to the amount of energy consumed by the system at the end of the day.

In 1996, T. G. Zimmerman and N. Gershenfeld realized that data could be sent using the human body as a transmission medium by modulating the electric field [1]. Depending on the terminology, the technology is known as intrabody communications, body channel communications, and human body communications (HBC). After 1996, research community has published hundreds of conference and journal papers about the topic. Also, the IEEE Std. 802.15.6-2012 includes a physical layer (PHY) option for HBC [2], which takes the HBC compliant commercial products one step closer to the market. HBC enables interesting new application possibilities: business cards can be exchanged by

* Correspondence: firstname.lastname@ee.oulu.fi
Centre for Wireless Communications, University of Oulu, Oulu, Finland

a handshake; secure doors can be opened without keys; and photo taken with a mobile phone can be printed just by touching a printer. It also addresses the problem of energy consumption for transferring data wirelessly since HBC operates at lower frequency bands which feature lower attenuation than the traditional wireless sensor and actuator network (WSAN) radio technologies, such as, e.g., ultra-wideband (UWB) and ZigBee.

Dozens of medium access control (MAC) protocols have also been proposed for WBANs [3, 4] and WSANs in order to make the wireless communication more energy efficient, robust, and reliable. Most of the protocols use duty cycling in order to save the energy in comparison with always-on approach. This means that a receiver node periodically switches (i.e., "cycles") between a low-power sleep mode and a receive mode. This approach reduces node's energy consumption, but there are also few drawbacks. First, a duty cycling node misses all the radio packets that are sent while it is in the sleep mode. This results in higher average message delivery latency and extra energy consumption for transmitters, which may have to repeat the packets multiple times. Second, the nodes still waste the energy for idle listening, i.e., useless channel listening when there are no incoming packets.

Wake-up receivers (WUR) have been designed to address the abovementioned problems. Typically, the WUR represents an additional simple and low-power radio receiver, which is integrated into a WBAN node as illustrated in Fig. 1. Low-power consumption enables to keep the radio in listen mode constantly, waiting for a pre-defined signal to activate the other electric circuits (e.g., sensing, communication, or signal processing) which stay in low-power mode. The prior studies [5, 6] have shown that WUR-based WBAN significantly outperforms the traditional duty cycle-based MAC approach in case of event-based communication, especially if the events occur rarely. The downside of the WURs is that the complexity of the node is increased because additional radio needs to be integrated. However, WUR solutions are relatively simple, and the complexity increase is not substantial.

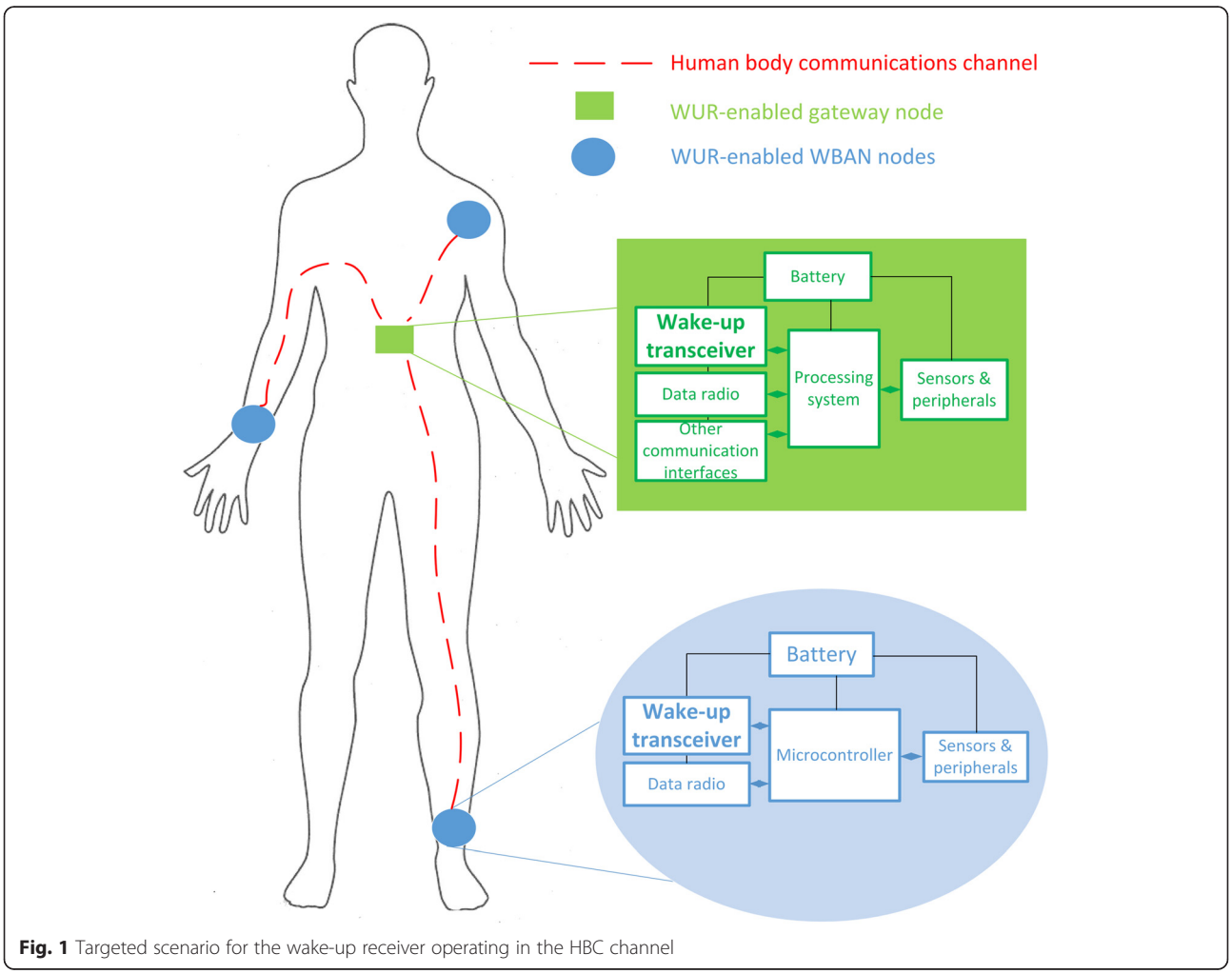

Fig. 1 Targeted scenario for the wake-up receiver operating in the HBC channel

The following basic application scenario is considered in this work. In Fig. 1, blue circle is a sensor node and a green rectangle is a gateway. Both devices are equipped with a WUR and a transmitter capable of transmitting a wake-up signal (wake-up transceiver). The node's sensors measure a certain physiological parameter while the gateway can keep all the power-consuming entities, except the WUR, in the sleep mode. When the node's sensor measures a value that exceeds a predefined threshold, the node transmits the wake-up signal to the gateway using HBC. Once the desired wake-up signal is detected, a microcontroller can activate a main data transceiver for acknowledgement and data communication purposes. On the other direction, the gateway can request data from the node by first sending the wake-up signal.

As this becomes clear from the above example, an efficient WUR needs to balance low energy consumption, provides sufficient communication range and the target signal detection reliability. Up to this point, several different receiver architectures have been employed for building the WURs [7]. For example, the architecture based on the superregenerative principle is known to provide good sensitivity at a cost of energy consumption. For instance, in [8], sensitivity of −100.5 dBm is achieved at the *bit error rate* (BER) of 10^{-3}, power consumption of 400 μW, and data rate of 5 kbps at 1.9 GHz band. To the best of the authors' knowledge, the lowest power consumption of a superregenerative WUR up to this date was achieved by the authors of [9]. The power consumption of that WUR is 42.5 μW at data rate of 100 kbps and the sensitivity reaches −72 dBm. In the current paper, we propose and report the design of an HBC-enabled WUR based on the superregenerative principle. In order to obtain the high sensitivity and selectivity while keeping the energy consumption low, the proposed solution employs self-quenching, uses loose synchronization method operating at sufficiently low (1.25 kbps) data rate. The real-life life experiments show that this enables our solution to achieve the sensitivity of −97 dBm for 10^{-3} BER while consuming 40 μW. This is the primary contribution of the current paper. The secondary contribution of this paper is the analysis of pros and cons of HBC, comparison of it with the other state-of-the-art (SotA) WBAN communication technologies, and the reported real-life measurement results related to the positioning of the electrodes for HBC communication.

The paper is organized as follows. First, in Section 2, we compare HBC against ZigBee, Bluetooth Smart, and ultra-wideband (UWB). A related work in the context of WURs is reported in Section 3. Section 4 reports the results of the experiments characterizing the path loss for HBC. Sections 5 and 6 report the details of the design and the evaluation of the proposed HBC-enabled WUR, respectively. Finally, Section 7 concludes the paper and summarizes the obtained results.

2 Comparison of low-power technologies for WBAN

Among all the wireless communication technologies available today on the market, there are three that are used often in WBANs. One of them is ZigBee, which has been on the market for a quite long period of time. The two others are the Bluetooth Low Energy (Bluetooth Smart), which is the low-power modification of the Bluetooth technology, and the impulse radio ultra-wideband (IR-UWB) which is targeting on the medical use cases among others. Table 1 summarizes the features

Table 1 A comparison of short-range wireless communication technologies suitable for WBAN

	HBC	ZigBee	Bluetooth Smart	Impulse radio—UWB
Standard	802.15.6-2012 [2]	802.15.4-2015 [57]	Bluetooth SIG[b] [58]	802.15.4-2015 [57] and 802.15.6-2012 [2]
Operating frequency	18.375–23.625 MHz	2.4–2.4835 GHz	2.4–2.485 GHz	<10.6 GHz with regulatory restrictions
Antenna/electrode size	1–2 cm (diameter)	3.1 cm ($\lambda/4$)	3.1 cm ($\lambda/4$)	5 cm × 5 cm ($\lambda_{3.1\ GHz}/2$)
Range	<3 m	<200 m	<100 m	<20 m
Over the air data rate	1.3125 Mbps	250 kbps	1 Mbps	0.11–27 Mbps
Interference to/from other devices	Low	High	High	Low
Power consumption in transmit mode	N/A commercially[a]	77.4 mW [59]	31.5 mW [60]	129 mW at 110 kbps [61]
Power consumption in receive mode	N/A commercially[a]	55.5 mW [59]	39.0 mW [60]	228 mW at 110 kbps [61]
Modulation	Frequency selective digital transmission	Direct sequence spread spectrum	Gaussian frequency shift keying	Pulse position modulation and phase shift keying

[a]802.15.6 compliant transceiver, e.g., introduced in [62] consumes 1.4 mW in transmit mode and 5.0 mW in receive mode
[b]Bluetooth Special Interest Group is responsible for standardization related issues

of all these technologies and of selected commercial implementations. As can be observed, HBC transceivers are operating in much lower frequencies than other wireless technologies. Lower operation frequency may enable to design transceivers that consume less power than transceivers in higher frequencies. In HBC, a transmitter couples with a body through capacitive coupling that creates a quasi-static electric field around the human body. Since the electric field stays close to the body, it gives two significant benefits. First, interference impact with other wireless devices is minor [10]. Second, it enhances security compared to traditional wireless technologies for WBAN by making the radio signal more difficult to eavesdrop.

In terms of communication range, the HBC is mostly limited to the surface of the user's body and thus can hardly have a path length exceeding few meters. For the other technologies, the communication distances of dozens to hundreds of meters under the line-of-sight condition can be reached. This can be used for integrating the WBAN with the other wireless networks operating in the environment.

One of the challenges at the moment of HBC technology is coupling the HBC transceiver and the user's body acting as communication media. In the SotA solutions, this is typically done by the means of electrodes and a special gel. Even though the connection may be good enough at the very beginning, as the time goes sweating and movement gradually makes the connection looser and the performance of communication can degrade. However, better attachment solutions are expected to emerge for electrodes when the HBC technology will be more mature. Also note that for some applications, especially the ones involving interactions with the off-body objects (e.g., a door handle or a printer), this issue may be not relevant.

3 Related work of wake-up receivers

Direct conversion architecture is common in wireless data receivers, but due to the challenges of DC offset and flicker noise, it has not been used in WUR solutions. The WUR solutions are based on variety of different receiver architectures [7]: matched filter [11], radio frequency envelope detection (RFED) [12–21], uncertain intermediate frequency (U-IF) [22, 23], sub-sampling [24, 25], superregenerative oscillator (SRO) [8, 9, 26], and injection locking [27–29]. The design involves many tradeoffs; therefore, it is not straightforward to define, which architecture is best suited for a WUR.

The RFED architecture has been the most popular approach to develop a WUR since it provides a straightforward way of power detection. In-band interference deteriorates the performance of the RFED-based approach. In contrast, a WUR that can detect spread spectrum signals is more robust against interference. To achieve low-power consumption, e.g., a passive surface acoustic wave matched filter can be utilized to despread the spreading coded wake-up signal. However, such a filter typically introduces large insertion losses. In the U-IF architecture, the uncertainty of the IF is caused by the use of low-power RF synthesizer that suffers from poor stability. Sensitivity of −88 dBm and power consumption of 50 μW is reported in [22]. Sub-sampling-based WUR proposed in [25] is based on a differential sample and hold (S&H) circuit. Even though the S&H circuit introduces high noise figure, −78 dBm sensitivity is achieved for 10 kbps data rate. In the SRO architecture, the received signal strength is detected by measuring oscillator's start-up times. The SRO-based receivers are typically very sensitive, but they consume more power than WURs based on other architectures. For example, in [8], a sensitivity of −100.5 dBm and 400 μW power consumption were reported. In injection locking-based architecture, the receiver couples with the carrier if the frequency is close to the oscillator's natural oscillation frequency.

The authors are aware of the three WUR solutions designed for the HBC and two of them are based on the injection-locking architecture [27, 28] and one on the SRO architecture [9]. In [27], it is proposed a WUR solution that is fabricated in a 1-mm^2 standalone chip with power consumption of 45 μW and sensitivity of −62 dBm. The design of the injection locked ring oscillator operating in the 45 MHz HBC band is reported in [28]. FSK-modulated input signal is locked with the ring oscillator, and then the signal is demodulated with a phase locked loop (PLL)-based demodulator. Frequency drift in the ring oscillator caused by temperature variations and leakage current is compensated using an auto frequency calibration method. The reported WUR implementation achieved the power consumption of 37.5 μW and has sensitivity of −62.7 dBm. The SRO in [9] has an RC resonator based on differential architecture, which is controlled by a 5-bit controlled current source. It operates in the 13.56 MHz frequency band, and it achieves sensitivity of −72 dBm with power consumption of 42.5 μW. WUR solutions that consume less than 50 μW are compared in Fig. 2 where the tradeoff between power consumption and sensitivity is illustrated clearly.

4 Human body communications

The quality of a HBC wireless link is affected by a variety of different factors: electrode material and size, operation frequency, coupling between the transceiver and the human body, distance between the transmitter and the receiver, size of the transmitter's and the receiver's ground planes, number of electrodes attached to a body, the body structure, body position, movement

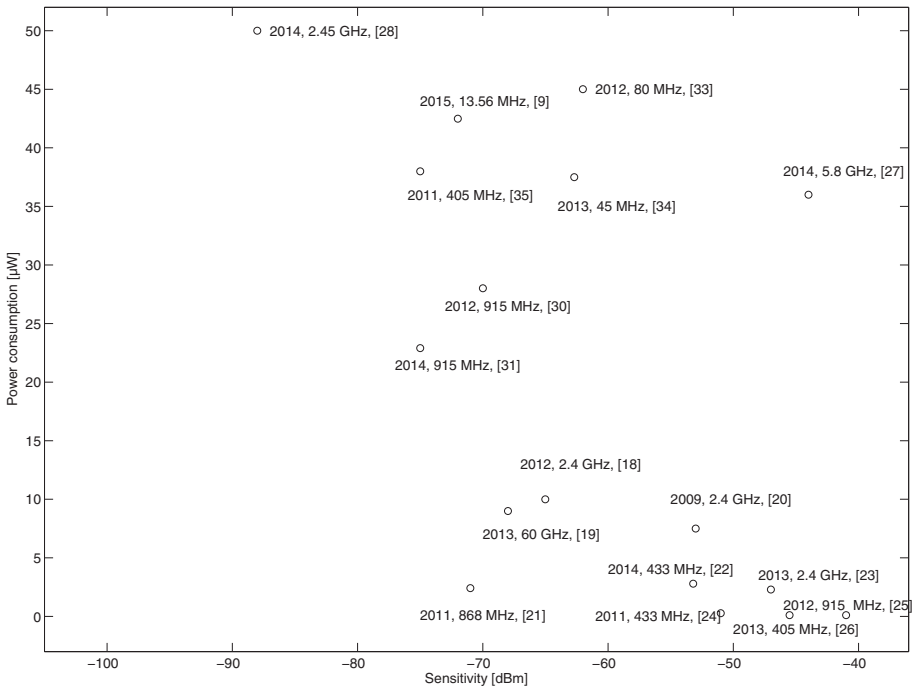

Fig. 2 Power consumption vs. sensitivity of state-of-the-art wake-up receivers

of a body, and impedance matching. Different electrode sizes are compared in [30]. It is noticed that the electrode resistance increases as the electrode size is decreased. The authors also report that there are significant differences between commercial electrodes even though they are made of same material (i.e., silver-silver chloride (Ag/AgCl)). HBC path loss models for different frequencies and distances are introduced, e.g., in [31, 32]. The path loss changes significantly as a function of frequency. The path loss at 21 MHz, which is the center frequency of IEEE Std. 802.15.6 HBC PHY, is around 36 dB at 1.2 m distance [32]. In [33], the authors note that the environment does not impact the channel characteristics.

The signal loop between a transmitter and a receiver is closed by a capacitive return path [31]. Thus, the ground plane size has an impact on the link quality. The impact of a transmitter's ground plane size is studied in [10], where it is reported that by doubling the size of the ground plane, S_{21}-parameter is increased by 3 dB. The human body starts to act as an antenna at higher frequencies. In [10], the electric field strength is measured in frequencies between 1 and 150 MHz. The measurement was repeated with different body structures (e.g., different heights). The electric field around the human body is strengthened as the frequency is increased, but there was variation between the different body types.

4.1 Dielectric properties of a human body

The human body is not uniform, i.e., it consists of different types of tissues that have unique dielectric properties. There is a commonly used online database [34], which provides the dielectric properties of body tissues at different frequencies. The database is based on results published in [35]. In Figs. 3, 4, and 5 are shown relative permittivity (ε_r), electrical conductivity (σ), and penetration depth (δ_p) in the frequency range of 20 to 45 MHz, respectively.

When a signal is induced to the human body, e.g., via an electrode, an electric field is originated around the human body (assuming that there are proper connections to ground). The electric field strength at a distance R from a charge Q can be derived from Maxwell's equations [36, 37] and it is given as

$$\vec{E} = \frac{Q}{4\pi\varepsilon R^2} = \frac{Q}{4\pi\varepsilon_r\varepsilon_0 R^2}, \quad (1)$$

where ε is permittivity, ε_r is the relative permittivity of the material (tissue in this context), and ε_0 is the electric constant (8.854×10^{-12} F/m). As can be seen, the relative permittivity of a tissue is inversely proportional to the electric field strength. However, the relative permittivity does not have an impact on the electric flux density, which describes how an electric field flows in this context through the human body as

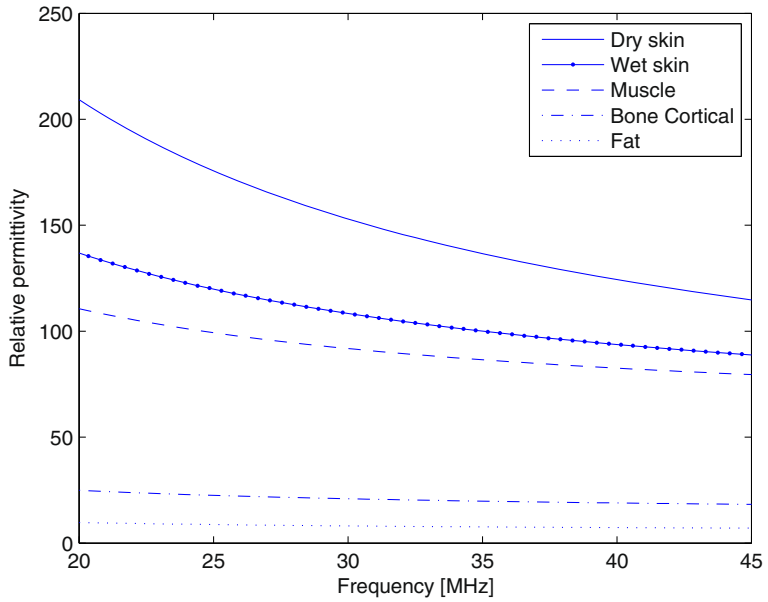

Fig. 3 Relative permittivity in different tissues (this graph is built based on data from [34])

$$\vec{D} = \varepsilon \vec{E} = \varepsilon_r \varepsilon_0 \vec{E} = \frac{Q}{4\pi R^2}. \quad (2)$$

4.2 Path loss with different electrode locations

Although in many HBC applications, an electrode is always connected to the skin or a conductive metallic plate touches the skin of a fingertip, we are interested on how tissues below the skin affect the electric field strength, and thus how much the communication performance is affected. As can be seen in Fig. 5, the electric field penetrates the skin; thus, the tissue beneath the skin is expected to have an impact on the electric field strength. Therefore, we measured the impact of electrode locations on the path loss. The electrode locations are chosen based on the tissue type beneath the dry skin. Tissues of interest are the same as used in Figs. 3, 4, and 5, i.e., the muscle, fat, and cortical bone. The measurement setup is shown in Fig. 6. The signal generator E4438C is used as a transmitter

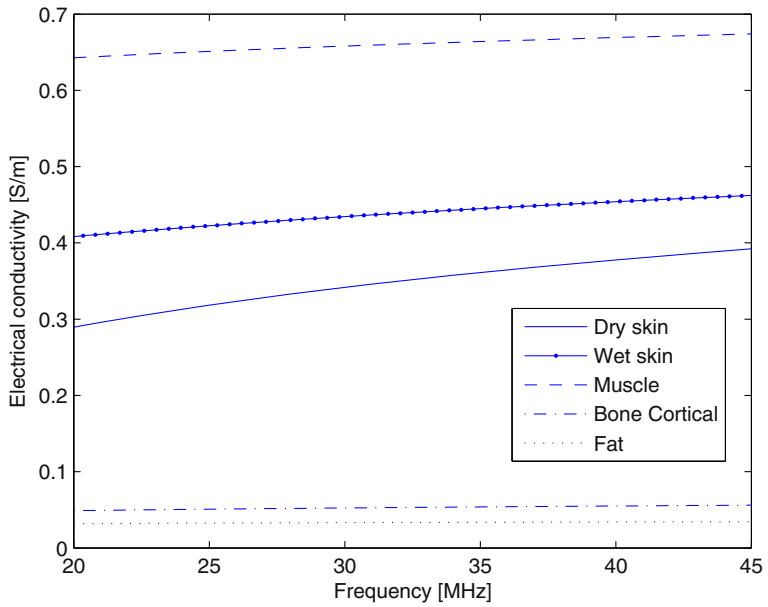

Fig. 4 Electrical conductivity in different tissues (this graph is built based on data from [34])

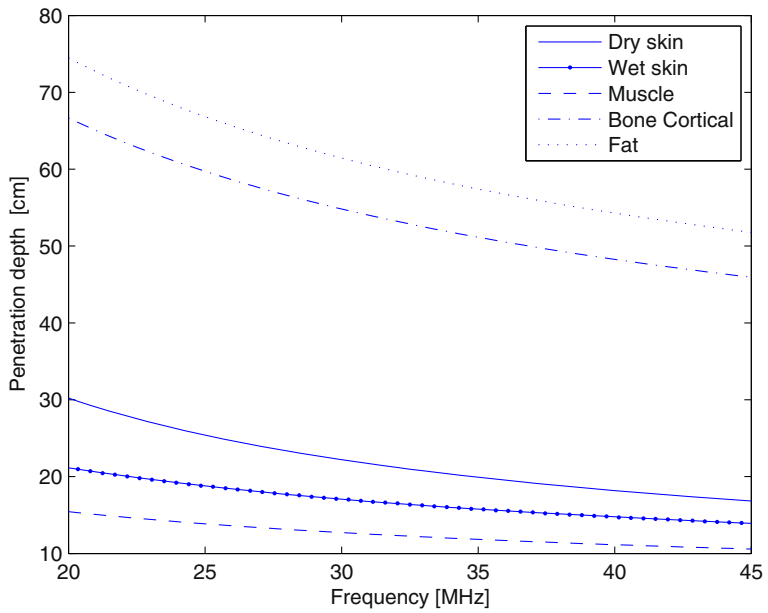

Fig. 5 Penetration depth is unique for each tissue (this graph is built based on data from [34])

(Tx) and spectrum analyzer as a receiver (Rx), and both devices are grounded. The electrodes are made of Ag/AgCl and are connected to the Tx and to the Rx via coaxial cables. The distance between the Tx and the Rx is kept fixed at 20 cm during the measurement campaign. The frequency of a continuous wave is changed from 20 to 45 MHz, and all the location combinations are measured, which are muscle-to-muscle, muscle-to-fat, muscle-to-bone, fat-to-fat, fat-to-muscle, fat-to-bone, and bone-to-bone.

The measured path losses for different cases are shown in Fig. 7. They clearly show that the location of the electrodes has large impact on the path loss. For instance, when both electrodes are attached to the dry skin above the fat, the path loss is 4–5 dB larger compared to the case when both electrodes are above the bone. The difference is significant and therefore the body composition needs to be taken into account when designing applications.

We also measured the path loss at different distances with three different frequencies. The path loss is shown in Fig. 8, which shows that the radio signal sustains substantial losses when coupled with the body, but the propagation over the body channel has very moderate losses and scales up slowly with the increase of the distance travelled. To give a practical example, at a 20-cm distance, the measured path loss for a 20 MHz signal was around 26 dB, which increased to about 34 dB at a distance of 1 m. For the air radio channel and a signal

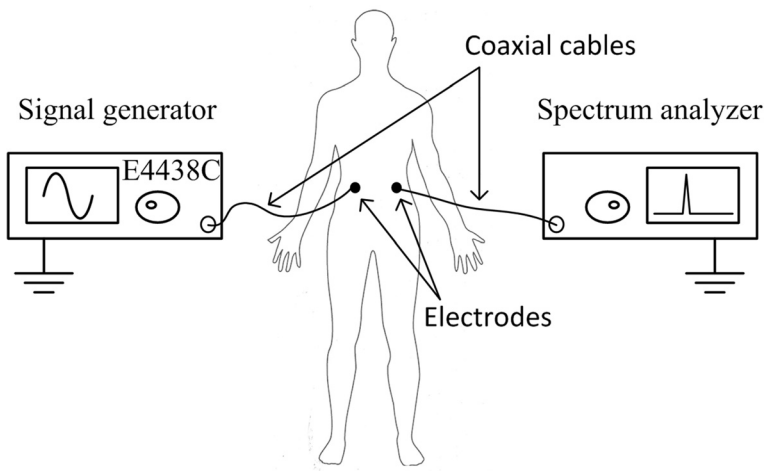

Fig. 6 Measurement setup for the path loss measurements with electrode locations from fat-to-fat

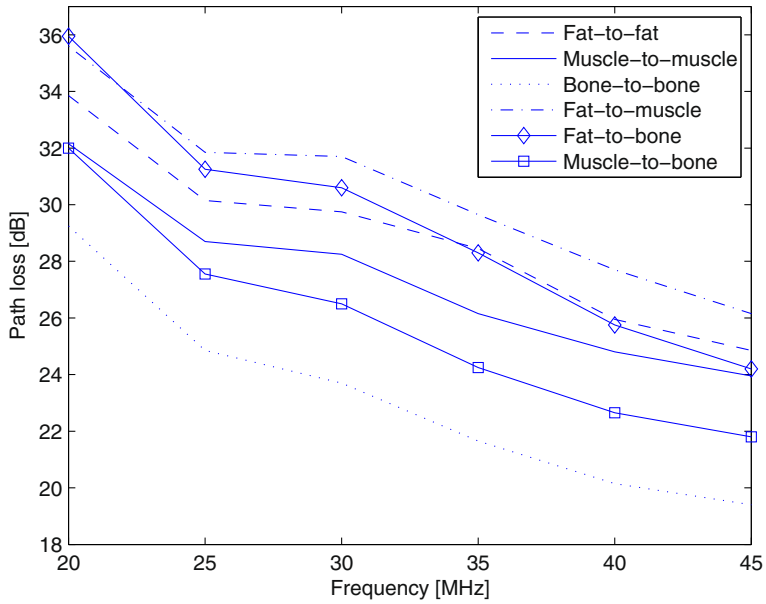

Fig. 7 The effect of the electrode position on the path loss for 20 cm HBC channel

of 2.4 GHz (e.g., BLE or ZigBee) according to the free space path loss

$$\mathrm{FSPL} = 10 \times \log_{10}\left(\frac{4\pi d}{\lambda}\right)^2, \quad (3)$$

where d is the distance and λ is the wavelength, one can expect the path loss of 26 dB at 20 cm and 40 dB at 1-m distance.

5 Superregenerative principle

In the core of a superregenerative receiver is a superregenerative oscillator (SRO) that was invented in 1922 by Edwin H. Armstrong [38]. The superregenerative receiver was superseded by superheterodyne receiver architecture (also invented by Armstrong in 1918) since it provided better performance in selectivity and data rate. Superregenerative architecture was brought back to very low-power receivers when integrated circuit (IC)

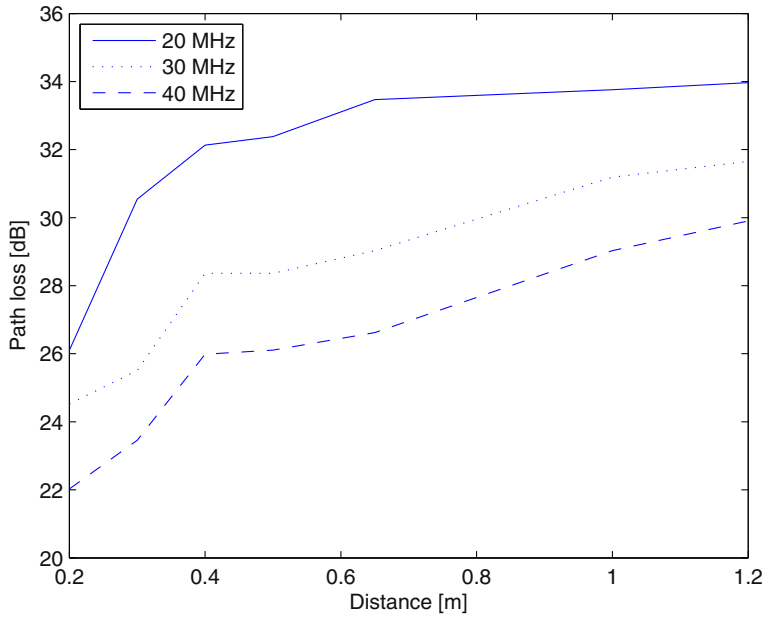

Fig. 8 The effect of the distance on the path loss for HBC channel

technologies provided sufficient performance and low-power capability. The principle of the superregenerative receiver operation is as follows. By a quench signal, the SRO is periodically switched between stable and unstable states. After going to unstable state, the SRO takes a sample of the signal coming from an electrode/antenna and starts oscillating. The start-up time depends on the magnitude of the incoming signal [39]. If the carrier is not present, the thermal noise is enough to start oscillations. Therefore, by measuring the SRO start-up time, one can define the strength of the incoming radio signal and demodulate, e.g., an amplitude-modulated signal. In the following subsection, the different components of a superregenerative WUR are discussed.

5.1 Superregenerative oscillator

Although many different superregenerative receiver designs have been proposed, the SRO, which is shown in Fig. 9, is well established and is very similar in most of them [40–43]. The SRO starts to oscillate when the transconductance (g) of the oscillator becomes negative. The transconductance is the sum of conductance of the LC tank (g_{LC}) and negative conductance ($-g_m/2$) provided by the two identical bipolar junction transistors, so $g = g_{LC} + (-g_m/2)$. If $g_m/2$ is smaller than g_{LC}, more current is needed to overcome the resistive losses in the LC tank. The minimum current needed to start oscillations is referred to as critical current (I_{crit}) which can be calculated as [43]

$$I_{crit} = 4U_T g_{LC}\frac{\beta+1}{\beta-1} = \frac{4C\omega_0 U_T}{Q_{LC}}\frac{\beta+1}{\beta-1}, \quad (4)$$

where $U_T = kT/q \approx 26$ mV is the thermal voltage at the temperature of operation, i.e., 300 K, k is the Boltzmann constant ($\approx 1.38 \times 10^{-23}$ J/K), q is elementary charge ($\approx 1.6 \times 10^{-19}$ C), β is transistor's base-collector current gain, C is the capacitance, ω_0 is oscillator's natural angular oscillation frequency, and Q_{LC} is the quality factor of the LC oscillator. In Fig. 10 is shown the effect of Q_{LC} on I_{crit} for three oscillation frequencies. It gives valuable information on how much bias current is required to enable oscillations and how the current scales with the increase of the operating frequency. It can be observed that at 28 MHz, I_{crit} does not decrease considerably when Q_{LC} exceeds 20. After that point, I_{crit} is well below 5 μA.

One of the practical issues related to the implementation of a superregenerative receiver operating at lower bands (i.e., 28 or 433 MHz) is the need of having high inductance and capacitance for the LC resonator. This may hamper the implementation as a single radio frequency integrated circuit (RFIC). For 868 MHz and low Q factors, the LC can be built on RFIC. However, with Q_{LC} of 10, I_{crit} is over 100 μA as shown in Fig. 11. With Q_{LC} of 30, which can be achieved with discrete components, I_{crit} is close to 50 μA.

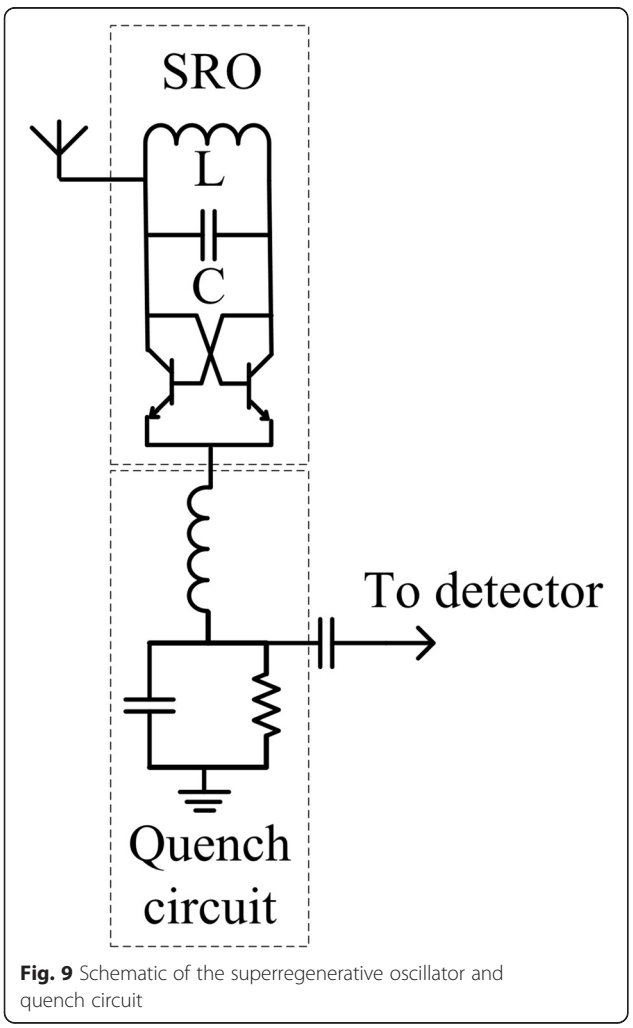

Fig. 9 Schematic of the superregenerative oscillator and quench circuit

5.2 Quench signal frequency, waveform, and generation

Quench signal has a major impact on superregenerative receiver's data rate, selectivity, and gain. It essentially defines the sampling rate of a superregenerative receiver. A sample is taken from the received signal after the quench signal allows oscillations to start. Then the amplitude of oscillations starts to increase exponentially (in the logarithmic mode) until the next quench signal resets them. This procedure is repeated continuously. Application requirements for data rate define the sufficient quench frequency.

The current consumption during the different phases of operation varies. To characterize this behavior and to estimate the total consumption as a part of the pre-study, we have first simulated the SRO and the quench circuit shown in Fig. 9 using the Advanced Design System.

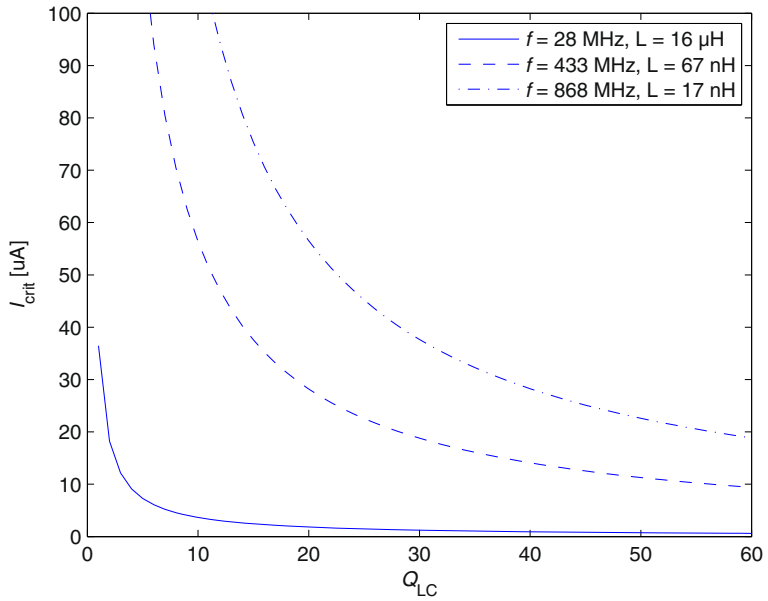

Fig. 10 Effect of Q_{LC} and oscillation frequency on critical current

Then we built a prototype and conducted practical measurements. In both cases, the Q_{LC} was 35, bias voltage was 1.5 V, quench frequency was 5.8 kHz, and oscillator's natural oscillation frequency was 28 MHz. Figure 12a illustrates the simulated amplitude of oscillations, and Fig. 12b shows the respective current consumption. From the presented results, one can clearly see that after the oscillations have started (in the depicted case by the noise, i.e., there is no carrier present at the input), their amplitude starts to increase to enable their easier detection. The latter causes the increase of the current consumption, which can be seen in Fig. 12b. At certain moment, the quench signal resets the oscillations, drawing the consumption down. The average current consumption for simulations and prototype measurements were 13 and 10 μA, respectively.

The quench signal waveform defines the receiver bandwidth and the superregenerative gain. In [44], the

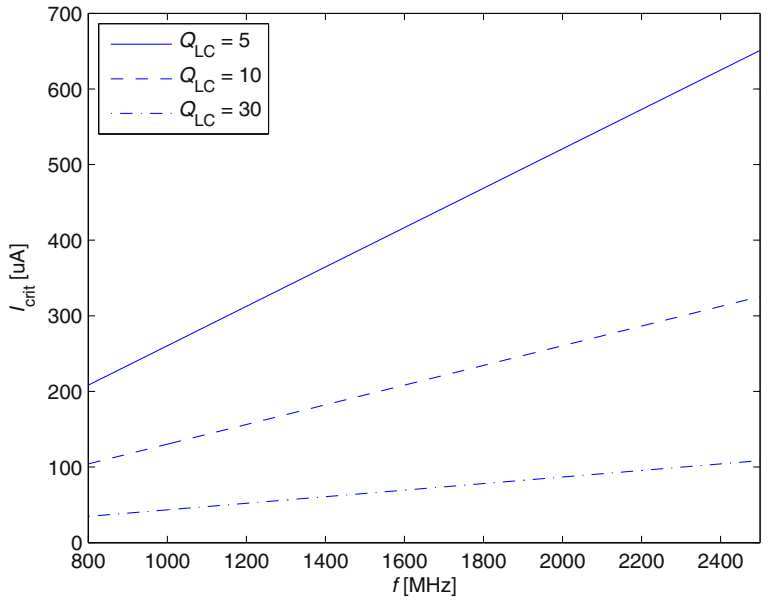

Fig. 11 Critical current in the 868 MHz (EU) and 915 MHz (US) and 2.4 GHz ISM bands with Q_{LC} of 5 and 10 achievable in RFIC and Q_{LC} of 30 with discrete components

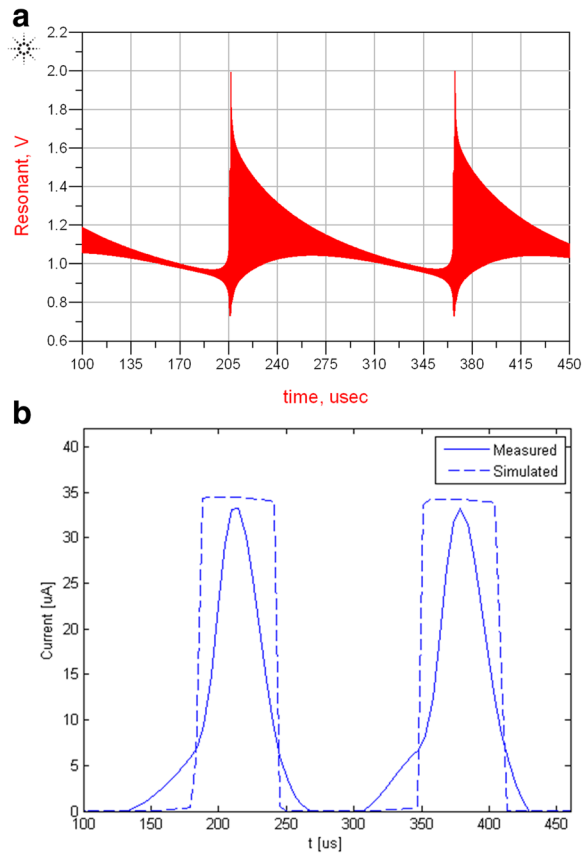

Fig. 12 **a** SRO's oscillations (simulated). **b** Current consumption at different SRO phases (simulated and measured)

authors have studied which quench waveform fits best for the different applications. They concluded that the square wave quench signal provides largest gain at the cost of selectivity. Triangular and saw-tooth quench signals provide better selectivity at the cost of gain. The bandwidth is determined by the change rate of transconductance during a sampling period as [45].

$$\mathrm{BW} = \frac{1}{\pi}\sqrt{\frac{1}{C}\frac{dg}{dt}}, \tag{5}$$

where g is transconductance. Therefore, if transconductance changes slowly during the sampling period, good selectivity will be achieved. A selectivity of the receiver is higher if data rate equals to the quench frequency [46]. However, to match quench frequency with data rate, one needs to enable accurate synchronization between a transmitter and a receiver. Unfortunately, such synchronization will require quite a lot of energy and is hardly feasible for WUR scenario. Our solution for solving this problem is detailed in the next section.

6 Superregenerative wake-up receiver

The proposed SWUR is designed to be used in energy-constrained WBAN nodes that utilize HBC channels. The major function of the receiver is to monitor the radio channel and to issue an interrupt for the MCU of the node once the wake-up signal with the proper address is received. The further data exchange relies on the main radio transceiver of the node. Additionally, the designed SWUR can be used by the MCU for sensing the radio channel before sending a wake-up message.

The high-level architecture of the receiver is depicted in Fig. 13. The designed SWUR consists of three major components, namely the SRO, the detector, and the digital logic that demodulates and processes the received wake-up code. Quench signal is used to control SRO oscillations and as the clock for the digital logic. For the SRO and the quench circuit, we used the very same solution as in Fig. 9.

As it was shown in the previous section, I_{crit} is well below 5 μA when Q_{LC} is over 20. The resonator is built with an inductor that has minimum Q-factor of 35. It means that only a small portion of power budget is consumed to enable oscillations. The bias current for the SWUR is fixed to a point above critical current where oscillations are stable and predictable in the presence of only noise. The bias current is fixed with a regulated bias voltage that is provided by the modular wireless sensor node platform [47, 48].

The digital part is implemented with Xilinx Coolrunner-II complex programmable logic device (CPLD) [49]. The current consumption of this device increases linearly with the frequency. The obvious drawback of reducing the quench frequency and the CPLD clock is the reduction of the data rate results in longer transmission time of the wake-up signal. However, since the wake-up codes are usually very short, we do not treat this to be the major issue.

6.1 Loose synchronization

The maximum allowed emission in the 21 MHz band (the HBC center frequency in the IEEE Std. 802.15.6) at 30 m distance from the transmitter measured in free space shall not exceed 30 μV/m [2]. The same applies for the 28 MHz band (SWUR operation band) [50]. Emissions at different distances can be calculated as [51]

$$E = \frac{\sqrt{30P_{\mathrm{TX}}}}{r}, \tag{6}$$

where P_{TX} is the transmit power and r is the radius of the communication range. Maximum transmit power can be calculated with different allowed emission levels as

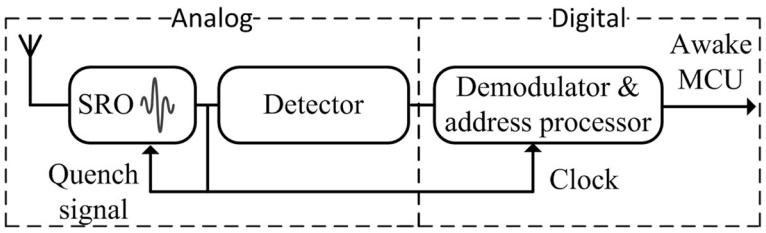

Fig. 13 High-level architecture of the proposed superregenerative self-quench wake-up receiver

$$P = \frac{E^2 r^2}{30}, \tag{7}$$

which gives maximum transmit power only −45.7 dBm. Very low allowed transmit power makes receiver sensitivity highly important metric for HBC receivers in order to enable that the wake-up range spans over the entire human body.

The noise floor of the receiver is dependent on bandwidth (BW) and receiver's noise figure (NF) as

$$P_{\text{noise\_floor}} = -174 + 10 \times \log_{10}(\text{BW}) + \text{NF}. \tag{8}$$

Minimizing the thermal noise floor is highly important for receivers that are based on power detection since it has major impact on the receiver sensitivity. Therefore, the SRO bandwidth should be matched with the wake-up signal bandwidth. It would decrease receiver noise floor, and there would be no need to put a band pass filter at the front-end, which would introduce additional insertion losses. However, this would require accurate synchronization.

In order to enable efficient reception of the WUR signal, we utilized the loose synchronization method which we proposed in [52]. The wake-up signal bits are pulse-width modulated (PWM) into the periods when radio carrier is absent (OFF-periods) which are separated by the short periods of carrier transmission (ON-periods) as illustrated in Fig. 14a. The long OFF-period is "1" bit and the short OFF-period corresponds to "0" bit.

The demodulation is accomplished in three stages. At first, the input signal is sampled by the SRO. Then, the output signal from the SRO is fed into the detector which compares the level of the signal with a predefined level thus making a decision about the presence of the carrier on the input. Finally, from the detector, the binary signal goes to the digital CPLD, which demodulates it by calculating the length of the OFF-period based on the number of SRO oscillations occurring between ON-periods (e.g., in the example illustrated in Fig. 14b four SRO oscillations occur during the long and two during short OFF-periods). Due to the lack of accurate synchronization, the signal may change from ON to OFF or vice versa during a sampling period that can cause fluctuations in the calculation of the period's length. To mitigate this effect, the digital logic takes into account the uncertainty intervals when measuring the period lengths.

6.2 Implementation

The prototype of the SWUR was designed using the computer-aided manufacturing (CAM) process with EAGLE printed circuit board (PCB) design software. The PCB board was manufactured at the University of Oulu workshop and assembled manually. The prototype is shown in Fig. 15. The dimensions of the SWUR prototype were selected to enable its integration with the modular wireless sensor node platform [47, 48] designed at the Centre for Wireless Communications, University of Oulu. The pins of the connector provide the power for the SWUR and enable it to wake-up the MCU. Note that of all the connector pins available, only two GPIO lines are currently utilized by the SWUR. The former one is used to wake up the microcontroller once

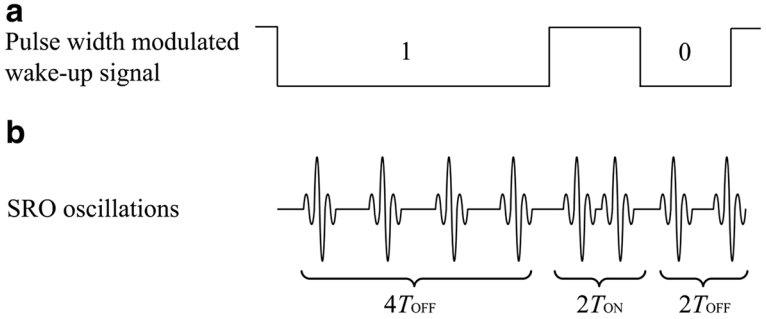

Fig. 14 **a** Modulated wake-up signal. **b** Number of oscillation periods in different stages

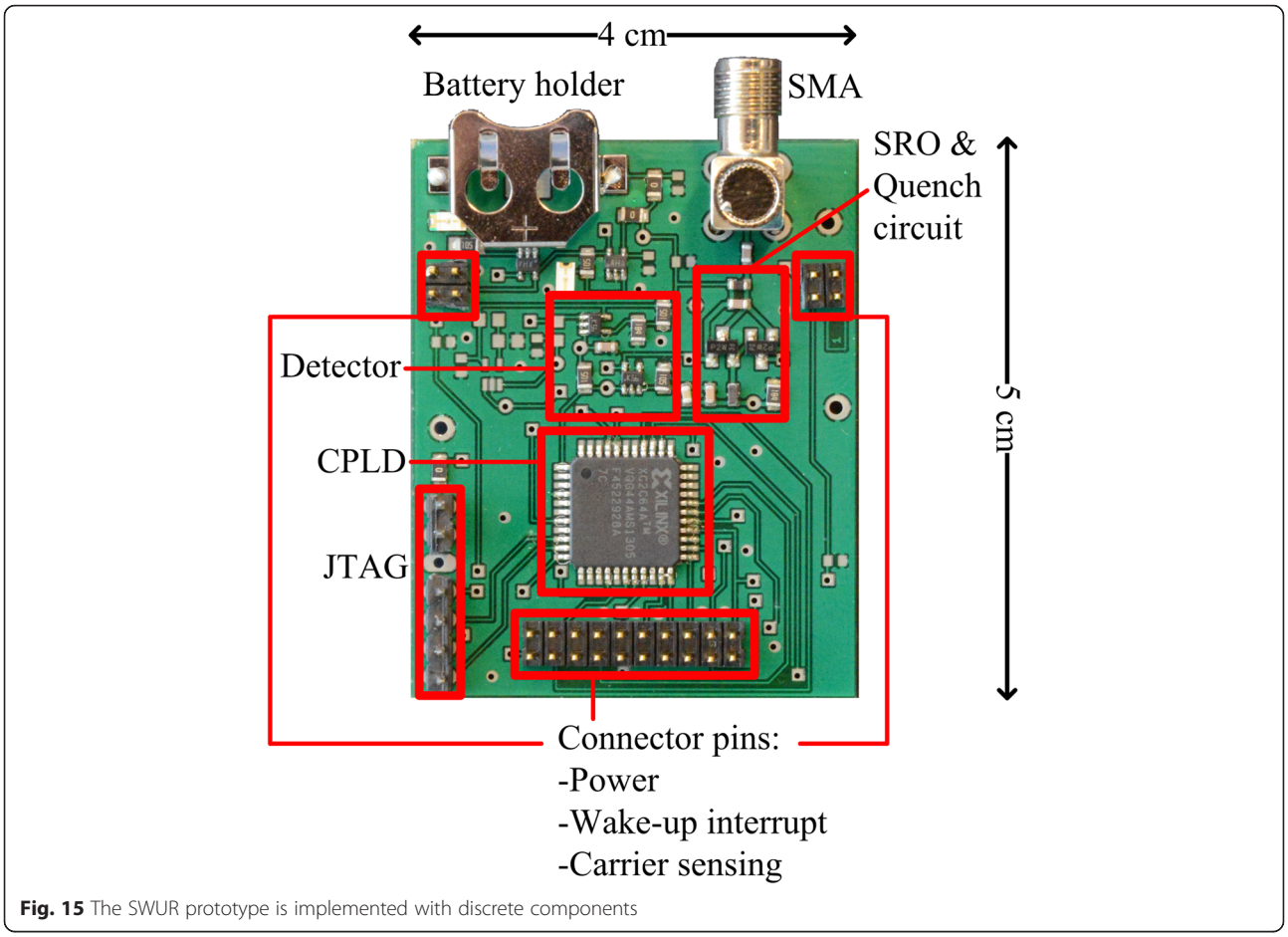

Fig. 15 The SWUR prototype is implemented with discrete components

the proper wake-up signal is detected and the latter one asserts if the level of the radio signal exceeds particular level. To enable programming the CPLD, the board was equipped with a JTAG connector. For enabling antenna attachment, the board is equipped with a SubMiniature type A (SMA) connector.

The SWUR operates in the 28 MHz. The operating voltage of the SWUR is 1.5 V. It can be powered with a coin-size battery, but due to the strict bias current requirements, the external stabilized voltage source is used in our test cases. The SRO is based on the wideband BFR92A bipolar junction transistors. The detector is built using a first-order low-pass filter and the TS881 comparators [53] which feature low current consumption (i.e., 210 nA) and can operate with 0.8 V supply voltage. The CPLD used for the wake-up code processing gives the flexibility to easily change the digital logic structure as well as the wake-up code without rebuilding the PCB.

Note that since the SRO is located at the front-end of the SWUR, the SotA superregenerative receivers (e.g., in [26, 46, 54, 55]) employ the isolation amplifier to amplify incoming signal and to prevent undesired emission from the SRO towards the electrode/antenna. In our design, this amplifier is intentionally omitted since we assume that the low SRO oscillation amplitudes may efficiently reduce the level of undesired emissions. To prove this in practice, we have conducted a set of real-life experiments which have confirmed our hypothesis. Namely, their results showed that the maximum power level of emissions of the designed SWUR towards the antenna/electrode does not exceed −75 dBm, which is well below the −57 dBm limit permitted for receivers operating in the 25 MHz–1 GHz band according to the frequency regulations [56]. In this respect, by omitting the amplifier, we not only make the design simpler, but also reduce the energy consumption of the SWUR.

6.3 Performance

There are three fundamental metrics which characterize the performance of a WUR, namely sensitivity, power consumption, and data rate. For the proposed solution, the latter is one of the design parameters and remains constant (equal to 1.25 kbps). The two other metrics have been measured using the developed hardware prototype.

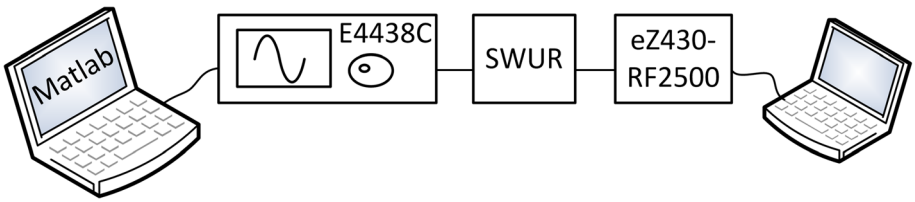

Fig. 16 Sensitivity measurement setup

For estimating the SWUR's power consumption, we used the Keysight's N6705B DC power analyzer with the N6781A module for accurate ultra-low-power consumption measurements (see Fig. 12b). The measured power consumption of the analog front-end and the programmable digital logic in the listening mode is 40 μW at 1.5 V supply. The measurements of the power consumption for the analog and digital sections showed that the power consumptions of both parts are about the same, i.e., 20 μW.

For measuring the sensitivity, we have used the measurement setup depicted in Fig. 16 and the test technique prescribed by ETSI in [56]. The test procedure gives the sensitivity level where 80 % of the packets are successfully received. The wake-up signal (a 5-bit packet containing a binary "10101" wake-up code) was generated with the Agilent E4438C vector signal generator, which was connected to the SWUR prototype via a coaxial cable. A Matlab script was used to trigger the generator. Every time the SWUR received the correct wake-up code, it generated a pulse which was detected by a pulse calculator, built using the TI's eZ430-RF2500, and reported to a laptop. The conducted experiments showed that the proposed SWUR has the sensitivity of −102 dBm. Note that in the current implementation, no mechanisms for correcting the errors and thus a single misinterpreted bit in the address code detection may prevent a wake-up or can cause a false wake-up. Therefore, the BER can be estimated from *packet error rate* (PER) using

$$\mathrm{BER} = 1-(1-\mathrm{PER})^{\frac{1}{n}}, \tag{9}$$

where n is the packet size in bits. This gives the BER of 4×10^{-2} for the designed SWUR at the sensitivity level of −102 dBm. Nonetheless, conventionally, the sensitivity is measured for the BER of 10^{-3}. Therefore, to enable more fair comparison of our results with the SotA works, we used the described above setup to measure the effect of the signal's power on the BER. The obtained results are illustrated in Fig. 17, from which one can see that the sensitivity of the proposed SWUR for the BER of 10^{-3} is about −97 dBm.

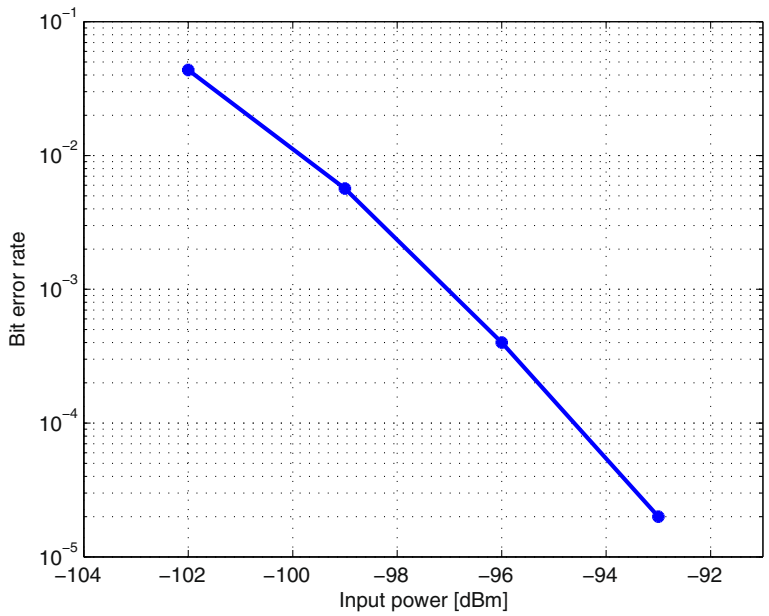

Fig. 17 Effect of the input power on the BER for the designed prototype

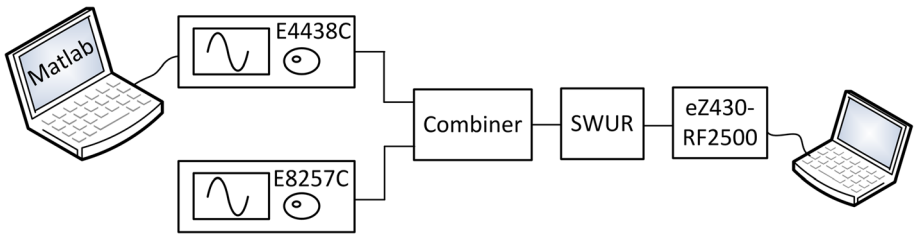

Fig. 18 Adjacent channel selectivity measurement setup

Finally, we also attempted to characterize the selectivity of the designed solution, which is a measure of capability of the receiver to reject the signals transmitted on the adjacent channels. For this purpose, we used the procedure detailed by ETSI in [56] and the setup illustrated in Fig. 18. The Agilent E4438C vector signal generator was used to generate the wake-up signal at the SWUR's central frequency. The second signal generator (Agilent E8257C) was generating an unmodulated carrier in a neighboring channel which is spaced 25 kHz from the wake-up channel. The two signals were combined using Mini-Circuit's ZFSC-2-1W-S combiner. We reduced the amplitude of the unmodulated adjacent channel signal to a level where SWUR still receives 80 % of the wake-up messages correctly. The measured adjacent channel selectivity is 44 dB.

6.4 Comparison of wake-up receivers for HBC

In Table 2, the parameters of the proposed SWUR are compared against the ones of the other HBC-enabled WURs. As one can see, the proposed SWUR is clearly the most sensitive, but it has the lowest data rate. High sensitivity means that lower transmit power can be used which reduces the radiation towards the human body. Alternatively, it also enables communication over higher distances (e.g., covering the whole body with less sensors). Multiple different performance metrics make the comparison of WURs quite nontrivial. For this reason, we propose the following figure-of-merit (FoM) that takes into account all three key metrics of WURs and the BER level where sensitivity value is obtained

$$\mathrm{FoM}(k_\mathrm{R}, k_\mathrm{S}, k_\mathrm{P}) = \frac{R}{S \times \mathrm{BER} \times P}, \tag{10}$$

where R is the data rate, S is the sensitivity in Watts, and P is the power consumption, k_R, k_S, and k_P are the respective weight coefficients which can be changed based on the requirements of the application (for our analysis we take $k_\mathrm{R} = k_\mathrm{S} = k_\mathrm{P} = 1$). The FoM is normalized here as

$$\eta = \frac{\mathrm{FoM}(R, S, P)}{\max(\mathrm{FoM}(R, S, P))}. \tag{11}$$

Another quite common metric used for comparing the receivers is the energy-per-bit, which takes into account power consumption and data rate, but not the sensitivity. The reported results in Table 2 show that even though due to the low data rate, the proposed solution is worse than the existing ones in terms of energy-per-bit, it outperforms the other solutions in the context of the proposed *FoM*.

7 Conclusions

Human body communications is an attractive alternative to the traditional WBAN radio technologies and can be used in a sheer diversity of medical and fitness applications. The major advantages of HBC compared to the traditional radio technology are threefold. First, the data traffic is alleviated from the air radio channels thus reducing the load on them. Second, since the electric field stays close to the body surface, the communication becomes more secure. Third, the lower attenuation at sub 100 MHz frequencies enables to use lower transmit power

Table 2 Comparison of addressing-enabled wake-up receivers for HBC

WUR	Operation frequency	Sensitivity	Power consumption	Data rate	Energy per bit	η
[9]	13.56 MHz	−62 dBm[a]	42.5 μW	100 kbps	0.43 nJ/b	0.0238
[27]	72/80 MHz	−62 dBm	45 μW	312 kbps	0.14 nJ/b	0.0702[b]
[28]	45 MHz	−62.7 dBm	37.5 μW	200 kbps	0.19 nJ/b	0.0634[b]
This work	28 MHz	−97 dBm[a]	40 μW	1.25 kbps	32.0 nJ/b	1

[a]BER = 10^{-3}
[b]BER not given, conventional 10^{-3} is assumed

in HBC. Nonetheless, HBC has also some limitations and restrictions. One of the most critical ones is the need for having good coupling between the HBC radio and the body. Therefore, in this work, we have investigated the effect of on-body position of the electrode on the attenuation of the HBC channel by the means of real-life experiments. The presented results show significant differences on the path loss between electrode positions due to the different dielectric properties of tissues. Also, the signal sustains substantial losses when coupled with the body but the propagation over the body channel has very moderate losses and scales up slowly with the increase of the distance travelled.

Motivated by this observation, in the second part of the paper, we propose a highly sensitive superregenerative wake-up receiver operating using HBC. The proposed receiver continuously listens for a pre-defined wake-up signal and on its reception activates the other electric circuitry (e.g., sensing, processing, and communication). The use of WURs can significantly reduce the energy consumption and increase the lifetime of the sensing applications. In the paper, we first discussed the principle of operation of the superregenerative receiver and it is shown using simulations which impact the different design parameters and solutions have on the performance of a superregenerative WUR. Then we presented and discussed in details our proposed solution, which employs self-quenching and loose synchronization method and operates at sufficiently low data rate (1.25 kbps). The proposed WUR has been first simulated and then implemented in a real-life prototype which has been thoroughly evaluated. The conducted measurement show that the WUR achieves the sensitivity of −97 dBm for 10^{-3} bit error rate while consuming 40 μW and features acceptable selectivity and emission level. Since the conventional metrics, such as energy-per-bit, does not enable to assess all the critical WUR parameters, we have proposed the new figure-of-merit which accounts for all the energy consumption, sensitivity, and the data rate of a WUR. Using the proposed metric, we have compared our proposed WUR with the state-of-the-art HBC WUR solutions. The results of comparison show that even though the proposed solution is worse than the existing ones in terms of energy-per-bit, it outperforms the other solutions when the sensitivity is also taken into account.

Acknowledgements
This work has been partially funded by the Finnish Scientific Advisory Board for Defence project EISIT (project number 2500 M-0043).

Authors' contributions
All the authors have contributed in various degrees to ensure the quality of this work. JP designed and implemented the proposed wake-up receiver, conducted the simulations, and the measurements. RV assisted with the wake-up receiver design, implementation, and measurements. KM and HK helped greatly in the writing process, and they also provided important feedback regarding wake-up receiver design. Finally, JI supervised the work. All authors read and approved the final manuscript.

Competing interests
The authors declare that they have no competing interests.

Received: 1 January 2016 Accepted: 12 July 2016
Published online: 03 August 2016

References

1. T. G. Zimmerman, Personal area networks: near-field intrabody communication. IBM systems journal, vol. 35, no. 3&4, (1996)
2. IEEE Std. 802.15.6–2012: IEEE standard for local and metropolitan area networks—Part 15.6: wireless body area networks. The Institute of Electrical and Electronics Engineers, Inc, Standard, pp. 1–271 (2012)
3. S Movassaghi, M Abolhasan, J Lipman, D Smith, A Jamalipour, Wireless body area networks: a survey. IEEE Communications Surveys & Tutorials **16**(3), 1658–1686 (2014)
4. E Kartsakli, A Lalos, A Antonopoulos, S Tennina, M Di Renzo, L Alonso, C Verikoukis, A survey on M2M systems for mHealth: a wireless communications perspective. Sensors **14**, 18009–18052 (2014)
5. H Karvonen, J Suhonen, J Petäjäjärvi, M Hämäläinen, M Hännikäinen, A Pouttu, Hierarchical architecture for multi-technology wireless sensor networks for critical infrastructure protection. Springer journal of Wireless Personal Communications **76**(2), 209–229 (2014)
6. H. Karvonen, J. Petäjäjärvi, J. Iinatti, M. Hämäläinen and C. Pomalaza-Ráez: A generic wake-up radio based MAC protocol for energy efficient short range communication. In proc. IEEE PIMRC Workshop: the Convergence of Wireless Technologies for Personalized Healthcare, Washington DC, USA, Sept. 2-5, 2014
7. J. Petäjäjärvi, H. Karvonen, K. Mikhaylov, A. Pärssinen, M. Hämäläinen and J. Iinatti: WBAN energy efficiency and dependability improvement utilizing wake-up receiver. IEICE Transactions on Communications, vol. E98-B, No. 04, (2015)
8. B. Otis, Y. H. Chee and J. Rabaey: A 400 μW-RX, 1.6 mW-TX super-regenerative transceiver for wireless sensor networks. In Proc. ISSCC, pp. 396–398, 2005. DOI: 10.1109/ISSCC.2005.1494036
9. H. Cho, H. Kim, M. Kim, J. Jang, J. Bae and H. J. Yoo: A 79 pJ/b 80 Mb/s full-duplex transceiver and a 42.5 μW 100 kb/s super-regenerative transceiver for body channel communication. IEEE journal of solid-state circuits, vol. 51, no. 1, (2016)
10. N Cho, J Yoo, S-J Song, J Lee, S Jeon, H-J Yoo, The human body characteristics as a signal transmission medium for intrabody communication. IEEE transactions on microwave theory and techniques **55**(5), 1080–1086 (2007)
11. S Tomabechi, A Komuro, T Konno, H Nakase, K Tsubouchi, Design and implementation of spread spectrum wireless switch with low-power consumption. IEICE transaction on fundamentals of electronics, communications and computer sciences **E84-A**(4), 971–973 (2001)
12. C. Kuang-Wei, L. Xin and J. Minkyu: A 2.4/5.8 GHz 10 μW wake-up receiver with −65/−50 dBm sensitivity using direct active RF detection. In proc. A-SSCC, pp. 337 – 340, 2012. DOI: 10.1109/IPEC.2012.6522694
13. T. Wada, M. Ikebe, E. Sano: 60-GHz, 9-μW wake-up receiver for short-range wireless communications. In proc. ESSCIRC, pp. 383–386, 2013. DOI: 10.1109/ESSCIRC.2013.6649153
14. M. S. Durante and S. Mahlknecht: An ultra low-power wakeup receiver for wireless sensor nodes. In proc. STA, pp. 167–170, 2009. DOI: 10.1109/SENSORCOMM.2009.34
15. C. Hambeck, S. Mahlknecht and T. Herndl: A 2.4 μW wake-up receiver for wireless sensor nodes with −71 dBm sensitivity. In proc. ISCAS, pp. 534 – 537, 2011. DOI: 10.1109/ISCAS.2011.5937620
16. G. U. Gamm, S. Stoecklin and L. M. Reindl: Wake-up receiver operating at 433 MHz. In proc. International Multi-Conference on Systems, Signals and Devices (SSD), pp. 1–4, Barcelona, Spain, 2014
17. E Nilsson, C Svensson, Ultra low-power wake-up radio using envelope detector and transmission line voltage transformer. IEEE Journal on Emerging and Selected Topics in Circuits and Systems **3**(1), 5–12 (2013). doi:10.1109/JETCAS.2013.2242777
18. SJ Marinkovic, EM Popovici, Nano-power wireless wake-up receiver with serial peripheral interface. IEEE Journal on Selected Areas in Communications **29**(8), 1641–1647 (2011)
19. N. E. Roberts and D. D. Wentzloff: A 98nW wake-up radio for wireless body area networks. In proc. RFIC, pp. 373–376, 2012. DOI: 10.1109/RFIC.2012.6242302
20. O. Seunghyun, N. E. Roberts and D. D. Wentzloff: A 116 nW multi-band wake-up receiver with 31-bit correlator and interference rejection. In proc. CICC, pp. 1–4, 2013. DOI: 10.1109/CICC.2013.6658500
21. J. Choi, I.-Y. Lee, K. Lee, S.-O. Yun, J. Kim, J. Ko, G. Yoon, S.-G. Lee: A 5.8-GHz DSRC transceiver with a 10-μA interference-aware wake-up receiver for the

Chinese ETCS. IEEE Trans. MTT, issue 99, pp. 1–15, 2014. DOI: 10.1109/TMTT.2014.2362118
22. C. Bryant, and H. Sjoland: A 2.45 GHz 50 uW wake-up receiver front-end with −88 dBm sensitivity and 250 kbps data rate. In proc. ESSCIRC, pp. 235–238, 2014.DOI: 10.1109/ESSCIRC.2014.6942065
23. N Pletcher, S Gambini, J Rabaey, A 52 μW wake-up receiver with −72 dBm sensitivity using an uncertain-IF architecture. IEEE Journal of Solid-State Circuits **44**(1), 269–280 (2009). doi:10.1109/JSSC.2008.2007438
24. S. Moazzeni, G.E.R. Cowan and M. Sawan: A 28 μW sub-sampling based wake-up receiver with −70 dBm sensitivity for 915 MHz ISM band applications. In proc. ISCAS, pp. 2797–2800, 2012. DOI: 10.1109/ISCAS.2012.6271891
25. S. Moazzeni, M. Sawan and G.E.R. Cowan: An ultra-low-power energy-efficient dual-mode wake-up receiver. IEEE Trans. on circuits and systems I: Regular papers, issue 99, pp. 1–10, 2014. DOI: 10.1109/TCSI.2014.2360336
26. J Ayers, K Mayaram, TS Fiez, An ultralow-power receiver for wireless sensor networks. IEEE Journal on Solid-State Circuits **45**(9), 1759–1769 (2010). doi:10.1109/JSSC.2010.2056850
27. B Joonsung, Y Hoi-Jun, A 45 μW injection-locked FSK wake-up receiver for crystal-less wireless body-area-network, in *In proc. Asian Solid-State Circuits Conference (A-SSCC)*, 2012, pp. 333–336
28. C. Hyunwoo, B. Joonsung and Y. Hoi-Jun: A 37.5 μW body channel communication wake-up receiver with injection-locking ring oscillator for wireless body area network. IEEE Transactions on Circuits and Systems I: Regular Papers, vol. 60, no. 5, pp. 1200–1208 (2013)
29. J. Pandey, J. Shi and B. Otis: A 120 μW MICS/ISM-band FSK receiver with a 44 μW low-power mode based on injection-locking and 9x frequency multiplication. In proc. ISSCC, pp. 460–462, 2011. DOI: 10.1109/ISSCC.2011.5746397
30. M. S. Wegmueller, M. Oberle, N. Felber and W. Fichtner: Signal transmission by galvanic coupling through the human body. IEEE Transactions on Instrumentation and Measurements, vol. 59, no. 4, (2010)
31. R Xu, H Zhu, J Yuan, Electric-field intrabody communication channel modeling with finite-element method. IEEE transactions on biomedical engineering **58**(3), 705–712 (2011)
32. J Bae, H Cho, K Song, H Lee, HJ Yoo, The signal transmission mechanism on the surface of human body for body channel communication. IEEE Transactions on Microwave Theory and Techniques **60**(3), 582–593 (2012)
33. Z Lucev, I Krois, M Cifrek, A capacitive intrabody communication channel from 100 kHz to 100 MHz. IEEE Transactions on Instrumentation and Measurements **61**(12), 3280–3289 (2012)
34. D. Andreuccetti, R. Fossi and C. Petrucci: An Internet resource for the calculation of the dielectric properties of body tissues in the frequency range 10 Hz–100 GHz. IFAC-CNR, Florence, Italy, 1997. Available online: http://niremf.ifac.cnr.it/tissprop/
35. C. Gabriel: compilation of the dielectric properties of body tissues at RF and microwave frequencies. Occupational and Environmental Health Directorate, Radiofrequency Radiation Division, Brooks Air Force Base, Texas, USA, (1996)
36. D. M. Pozar: Microwave Engineering, 4th edition, John Wiley & Sons, (2011)
37. JC Maxwell, A dynamical theory of the electromagnetic field. Philosophical Transactions on Royal Society Publishing **155**, 459–512 (1865)
38. EH Armstrong, Some recent developments of regenerative circuits, in *In proc. Institute of Radio Engineers*, 1922, pp. 244–260
39. F.W. Frink: The basic principles of super-regenerative reception. In proc. Institute of Radio Engineers, Vol. 26, no. 1, (1938)
40. A Vouilloz, M Declercq, C Dehollain, A low-power CMOS super-regenerative receiver at 1 GHz. IEEE Journal of Solid-state Circuits **36**(3), 440–451 (2001)
41. N Joehl, P Favre, P Deval, A Vouilloz, C Dehollain, M Declercq, A BiCMOS mircopower 1 GHz super-regenerative receiver, in *proc. ISSSE*, 1998, pp. 74–78
42. E. Insam, Designing super-regenerative receivers. Electronics World, (2002)
43. A Vouilloz, M Declercq, C Dehollain, Selectivity and sensitivity performances of superregenerative receivers, in *proc. Circuits and Systems*, vol. 4, 1998, pp. 325–328
44. P Favre, N Joehl, A Vouilloz, P Deval, C Dehollain, M Declercq, A 2-V 600-μA 1-GHz BiCMOS super-regenerative receiver for ISM applications. IEEE Journal of Solid-state Circuits **33**(12), 2186–2196 (1998)
45. G. G. Macfarlene and J. R. Whitehead: The super-regenerative receiver in the linear mode. In proc. Institution of Electrical Engineers, vol. 93, Part IIIA, p. 284–286 (1946)
46. F. X. Moncunill-Geniz, P. Palà-Schönwälder, C. Dehollain, N. Joehl and M. Declercg: An 11-Mb/s 2.1 mW synchronous superregenerative receiver at 2.4 GHz. IEEE Transactions on Microwave Theory and Techniques, vol. 55, no. 6, (2007)
47. K. Mikhaylov, J. Petäjäjärvi, M. Mäkeläinen, A. Paatelma, T. Hänninen, Demo-modular multi-radio wireless sensor platform for IoT trials with Plug&Play module connection. Annual International Conference on Mobile Computing and Networking (MobiCom), pp. 188-189, (2015)
48. K Mikhaylov, J Petäjäjärvi, M Mäkeläinen, A Paatelma, T Hänninen, Extensible modular wireless sensor and actuator network and IoT platform with Plug&Play module connection, in *In proc. IPSN*, 2015, pp. 386–387
49. Xilinx: XC2C64A CoolRunner—II CPLD. Datasheet, (2008)
50. Federal Communications Commission: understanding the FCC regulations for low-power, non-licensed transmitters. https://transition.fcc.gov/Bureaus/Engineering_Technology/Documents/bulletins/oet63/oet63rev.pdf. Accessed May 28 2016
51. International Telecommunication Union: Recommendation ITU-R P.525-2–Calculation of free-space attenuation. https://www.itu.int/dms_pubrec/itu-r/rec/p/R-REC-P.525-2-199408-I!!PDF-E.pdf. Accessed May 17, 2016
52. J. Petäjäjärvi, K. Mikhaylov, H. Karvonen, R. Vuohtoniemi and M. Hämäläinen: Loose synchronization method for low-power superregenerative wake-up receiver. In proc. ISMICT, pp. 1–4, March, 2015
53. FX Moncunill-Geniz, P Palà-Schönwälder, J Bonet-Dalmau, F Del Aguila López, R Giralt-Mas, *Ultra Wideband Impulse Radio Superregenerative Reception. Ultra Wideband Communications: Novel Trends–System, Architecture and Implementation*, 2011
54. STMicroelectronics: Rail-to-rail 0.9 V nanopower comparator. Datasheet, (2013)
55. JP Carmo, JC Ribeiro, PM Mendes, K Correia, Super-regenerative receiver at 433 MHz. Journal of Microelectronics **42**(5), 681–687 (2011)
56. ETSI Electromagnetic compatibility and radio spectrum matters (ERM), short range devices (SRD), radio equipment to be used in the 25 MHz to 1 000 MHz frequency range with power levels ranging up to 500 mW, Part 1: Technical characteristics and test methods, EN 300 220-1 (2012)
57. IEEE Std. 802.15.4-2015: Approved draft standard for low-rate wireless personal area networks (WPANs). IEEE P802.15.4-REVc/D01, pp. 1–702, (2015)
58. Bluetooth Special Interest Group. Available online: https://www.bluetooth.com/
59. Texas Instruments: CC2520, 2.4 GHz IEEE 802.15.4/ZIGBEE RF transceiver. Datasheet, Dec. 2007
60. Nordic Semiconductor: Multiprotocol Bluetooth low energy/2.4 GHz RF system on chip. Datasheet, 2014
61. Decawave: IEEE802.15.4-2011 compliant ultra-wideband (UWB) low-power low-cost IC transceiver. Datasheet v. 2.04, 2014
62. H. Cho, H. Lee, J. Bae and H. J. Yoo: A 5.2 mW IEEE 802.15.6 HBC Standard compatible transceiver with power efficient delay-locked-loop based BPSK demodulator. IEEE journal of solid-state circuits, vol. 50, no. 11, Nov. 2015